

**Molecular dynamics simulation of disordered zircon**

R. Devanathan,\* L. R. Corrales, and W. J. Weber

*Pacific Northwest National Laboratory, P.O. Box 999, Richland, Washington 99352, USA*

A. Chartier and C. Meis

*CEA-Saclay INSTN/UEPEM Bât. 395, 911191 Gif-Sur-Yvette, France*

(Received 18 September 2003; revised manuscript received 1 December 2003; published 27 February 2004)

The melting of zircon and the amorphous state produced by quenching from the melt were simulated by molecular dynamics using a partial charge model combined with the Ziegler-Biersack-Littmark potential. The model has been established for the description of the crystalline and aperiodic structures of zircon in order to be used for the simulation of displacement cascades. It provides an excellent fit to the structure, and accounts with convenient precision for the mechanical and thermodynamic properties of zircon. The calculated melting temperature is about 2100 K. The activation energy for self-diffusion of ions in the liquid state was determined to be 190–200 kJ/mole. Melt quenching was employed to produce two different disordered states with distinct densities and structures. In the high density disordered state, the zircon structure is intact but the bond angle distributions are broader, 4% of the Si units are polymerized, and the volume swelling is about 8%. In the low density amorphous state, the Zr and Si coordination numbers are lower, and the Zr-O and Si-O bond lengths are shorter than corresponding values for the crystal. In addition, a highly polymerized Si network, with an average connectivity of 2, is observed in the low density amorphous state. These features have all been experimentally observed in natural metamict zircon. The present findings, when considered in light of experimental radiation effects studies, suggest that the swelling in zircon arises initially from disorder in the zircon crystal, and at high doses the disordered crystal is unable to accommodate the volume expansion and transforms to the amorphous state.

DOI: 10.1103/PhysRevB.69.064115

PACS number(s): 61.43.-j, 64.70.-p, 66.10.-x, 31.15.Qg

**I. INTRODUCTION**

Zircon ( $\text{ZrSiO}_4$ ) is a promising ceramic host material for the disposition of high-level nuclear waste and the immobilization of excess weapons plutonium.<sup>1,2</sup> It occurs in nature with U and Th concentrations of up to 5000 ppm, and exhibits high resistance to physical and chemical degradation. Zircon has also been observed to be an important actinide-bearing phase in the crystallized core melt of the Chernobyl Nuclear Power plant.<sup>3</sup> As an actinide bearing phase, natural  $\text{ZrSiO}_4$  undergoes self-radiation damage from  $\alpha$  decay leading to an aperiodic or amorphous state known as the metamict state. The  $\alpha$ -decay event releases a high energy (4–6 MeV)  $\alpha$  particle that dissipates its energy mostly by electronic energy loss processes and an energetic recoil nucleus of about 0.1 MeV that slows down by creating an atomic displacement cascade.<sup>4</sup> An understanding of radiation effects in crystalline zircon and a determination of the structure of the aperiodic state are essential to ensure the reliability of zircon and related ceramics for nuclear waste disposition. Furthermore, interest in amorphous zircon is driven by the fact that amorphous zirconium silicates are candidates to replace  $\text{SiO}_2$  as the gate dielectric material in sub-0.1  $\mu\text{m}$  complementary metal-oxide semiconductor technology.<sup>5</sup>

The accumulation of  $\alpha$ -decay damage in zircon over geologic time scales ( $\sim 570$  million years) has been extensively studied because of its importance to geochronology. In addition, studies of equivalent radiation effects, accumulated over two decades, in Pu-doped zircon and ion-irradiation effects in synthetic zircon have shed light on the effects of irradiation dose, temperature and ion mass on the loss of

crystalline periodicity of zircon (Ref. 4, and references therein). The volume change associated with the crystalline to amorphous transition was found to be about 18%.<sup>4,6</sup> However, there is considerable disagreement regarding the mechanism of amorphization.<sup>4,7,8</sup> Moreover, the atomistic details of damage accumulation and recovery in zircon are not well understood.

The structure of metamict zircon has also been examined by a series of experiments. Vance<sup>9</sup> studied the infrared (IR) spectra from natural zircon and concluded that the Si-O bonding was similar to that in vitreous  $\text{SiO}_2$ , but found no evidence for phase separation into  $\text{SiO}_2$  and  $\text{ZrO}_2$ . A subsequent study<sup>10</sup> using IR spectroscopy concluded that the structure of metamict zircon consists of distorted and disoriented isolated silica tetrahedra and that the immediate environment of  $\text{Zr}^{4+}$  ion is highly disturbed with variation in Zr-O bond distances and Zr-O-Si bond angles. Farges and Calas<sup>11</sup> used x-ray absorption spectroscopy (XAS) to determine that the  $\text{Zr}^{4+}$  coordination number in metamict zircon is reduced from eight to seven in crystalline zircon and that the Zr-O bond length contracts by about 0.1 Å in the metamict state. The study suggests that a further contraction of the Zr-O bond length by 0.02 Å, which may occur at high radiation doses, could lead to six-coordinated  $\text{Zr}^{4+}$ . A recent Raman spectroscopy study<sup>12</sup> of natural zircon samples concluded that  $\text{ZrO}_2$  and  $\text{SiO}_2$  are not the principal products of metamictization and that the  $\text{SiO}_4$  tetrahedra are less polymerized than those in silica. Farnan and Salje<sup>13</sup> used  $^{29}\text{Si}$  nuclear magnetic resonance (NMR) to probe local structure in natural zircon. They observed an average polymerization of two to three bridging oxygens per  $\text{SiO}_4$  tetrahedra in metamict

zircon, and suggest that a large number of interstitial defect oxygen sites may be present in the amorphous phase. This metamict state has been claimed to result from quenching of a molten state due to a thermal spike in the displacement cascade.<sup>14</sup> In contrast to these studies, Begg *et al.*<sup>6</sup> have observed by XAS and x-ray diffraction (XRD) that the amorphous structure of synthetic zircon containing 8.85 wt. % <sup>238</sup>Pu, subjected to accelerated  $\alpha$ -decay damage over 18 years, was lacking in long-range order, but retained a distorted zircon structure with rotated SiO<sub>4</sub> and ZrO<sub>8</sub> polyhedra and zircon stoichiometry over length scales up to 0.5 nm. There is a pressing need to interpret these experimental results using atomic level simulations of damage accumulation and to compare the structure of metamict zircon to that of melt-quenched zircon.

In an attempt to elucidate the atomistic details of damage accumulation and recovery processes in zircon, several computer simulations have been performed recently.<sup>15–19</sup> Despite the fact that classical molecular dynamics (MD) simulations do not account for electronic effects, MD is ideally suited for the small time (ps) and distance (10 nm) scales associated with the dynamics of primary damage in zircon. MD simulations of radiation damage processes in ceramics are generally limited by the availability of reliable interatomic potentials to describe the complex interactions in oxide systems, the demands on computation time arising from the long range of the Coulombic interaction, and the nonequilibrium nature of the simulations that preclude the use of shell-model potentials found in the literature<sup>20–21</sup> as well as charge transfer techniques that are far from reliable at present.

In the present work, the melting of zircon and structure of the amorphous state produced by melt quenching have been examined using a partial charge interatomic potential model developed at the CEA-Saclay. This model gives a quite satisfactory fit to the equilibrium structure and elastic constants of zircon. In addition, it reproduces the thermal decomposition of zircon at a temperature comparable to the experimental value and provides diffusion coefficients in the liquid state that are in general agreement with experimental values for silicate melts. Two different disordered states with volume swelling of about 8 and 18 % have been simulated. The results provide insights into the structure of amorphous zircon, and are in broad agreement with experimental observations and a recent *ab initio* molecular dynamics study.<sup>19</sup>

## II. DETAILS OF THE SIMULATION

### A. Interionic potential model

The interaction between the ions in zircon was modeled using the Coulomb potential given by

$$V_{ij}^C = \frac{q_i q_j e^2}{4 \pi \epsilon_0 r_{ij}}, \quad (1)$$

where  $q_i$  and  $q_j$  are the charges of the ions interacting at a distance  $r_{ij}$ ,  $e$  is the electron charge, and  $\epsilon_0$  is the vacuum permittivity. This interaction was evaluated using the smooth particle mesh Ewald method.<sup>22</sup> At distances less than 10 Å,

TABLE I. Born-Mayer potential parameters for ZrSiO<sub>4</sub>.

Interactions	$A_{ij}$ (eV)	$\rho_{ij}$ (Å)	Charges
Zr-O	1967.0	0.305004	Zr: +3.8
Si-O	1277.0	0.227225	Si: +2.0
O-O	1755.0	0.306820	O: -1.45

an additional interaction was included for Zr-O, Si-O, and O-O pairs in the form of a Born-Mayer potential given by

$$V_{ij}^B = A_{ij} \exp\left(-\frac{r_{ij}}{\rho_{ij}}\right). \quad (2)$$

The parameters  $A_{ij}$  and  $\rho_{ij}$  for the three interactions, and the charges  $q$  for the Coulomb potential are given in Table I. The model parameters, including the ion charges, were determined by fitting to the structure, elastic constants, and dielectric properties of crystalline zircon. The specific heat  $C_p$  and entropy  $S$  have not been included in the fitting. To be transferable to nonbulk crystalline phases and surfaces, further refinement of the potential is needed. The potential parameters were optimized using the GULP code<sup>23</sup> by minimizing the sum of squares of the differences between calculated and experimental values of the fitted properties.

For radiation damage studies, it is important to model the nuclear stopping accurately, by using a realistic repulsive potential. At distances much less than the equilibrium interionic separation, the Born-Mayer potential is joined smoothly to the repulsive Ziegler-Biersack-Littmark (ZBL) potential<sup>24</sup>  $\Phi_{ij}$  using the Fermi function  $F(r_{ij})$  to give an effective short-range interaction of  $FV_{ij}^B + (1-F)\Phi_{ij}$ . The ZBL potential is a screened Coulombic repulsion between nuclei with a universal screening function fitted to a large number of atom pairs and has the form

$$\Phi(x) = 0.1818e^{-3.2x} + 0.5099e^{-0.9423x} + 0.0.2802e^{-0.4029x} + 0.02817e^{-0.2016x}, \quad (3)$$

where

$$x = \frac{r_{ij}(Z_1^{0.23} + Z_2^{0.23})}{0.8854a_0}. \quad (4)$$

$a_0$  is the Bohr radius and  $Z_1$  and  $Z_2$  are the atomic numbers of the two atoms interacting at distance  $r_{ij}$ .

The Fermi function is given by

$$F(r_{ij}) = \frac{1}{1 + \exp(-b_f[r_{ij} - r_f])}. \quad (5)$$

The parameters  $b_f$  and  $r_f$  were chosen to ensure that the potential and its derivative are continuous and monotonic for all values of  $r_{ij}$ . The parameters of the Fermi function are given in Table II. The effective short range potential energy is shown in Fig. 1 for Zr-O, Si-O, and O-O interactions. The potential and its derivative were found to be finite, single valued and continuous for the range of values of  $r_{ij}$  relevant to the simulation. The effective short-range potentials for all interactions were read from a table.

TABLE II. Fermi function parameters for  $\text{ZrSiO}_4$ .

Interactions	$b_f(\text{\AA}^{-1})$	$r_f(\text{\AA})$
Zr-Zr	6.0	1.00
Zr-Si	6.0	1.00
Zr-O	6.0	0.87
Si-Si	6.0	1.00
Si-O	6.0	0.62
O-O	6.0	0.30

Table III compares the lattice parameters, unit cell volume, bond lengths and bond angles from the present model of zircon to those obtained by experiment.<sup>25</sup> The fit to the structural properties of zircon is excellent. The relative stability of  $\text{ZrSiO}_4$  in the zircon and reidite structures, shown in Fig. 2, was also evaluated to test the reliability of the potential. Reidite is a high pressure polymorph of zircon found in upper Eocene impact ejecta layer in marine sediments and produced by shock loading of zircon at 30–50 GPa.<sup>26</sup> Both zircon (space group  $I4_1/amd$ ) and reidite (space group  $I4_1/a$ ) are tetragonal. The density of reidite is about 11% larger and the potential energy at 300 K (in the constant NVT ensemble) is about 133 kJ/mol higher than the corresponding values for zircon. The present model stabilizes the correct polymorph of zircon at 300 K.

Table IV compares the elastic constants, thermodynamic properties, and static dielectric constant of zircon from experiment<sup>27–33</sup> and the present work. Matching the experimentally determined elastic constants and thermodynamic properties is essential to correctly model the response of the system to strains produced in the displacement cascade as well as the subsequent relaxation process. The present model is able to reproduce the equilibrium elastic constants, specific heat, entropy (calculated in the primitive unit cell with 32  $k$  points along the Brillouin zone), and static dielectric constant of crystalline zircon as well as vibrational entropy up to 1800 K as shown in Fig. 3.

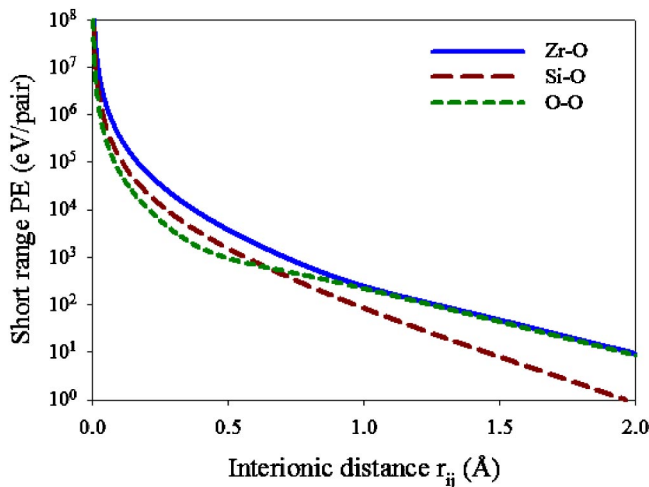


FIG. 1. The effective short range potential energy of the Zr-O, Si-O, and O-O interactions as a function of distance.

TABLE III. Zircon structural parameters from experiment and the present model.

Property	Experiment (Ref. 25)	Present model
Unit cell volume ( $\text{\AA}^3$ )	261.1	265.6
Lattice constant $a$ ( $\text{\AA}$ )	6.607	6.602
Lattice constant $c$ ( $\text{\AA}$ )	5.982	6.093
Si-O bond length ( $\text{\AA}$ )	1.622	1.637
Zr-O bond lengths ( $\text{\AA}$ )	2.131	2.129
	2.268	2.297
O-O bond lengths ( $\text{\AA}$ )	2.430	2.430
	2.494	2.531
	2.752	2.786
	2.842	2.854
	3.071	3.071
O-Si-O bond angles	97.0°	97.0°
	116.1°	116.0°
O-Zr-O bond angles	64.8°	63.8°
	80.4°	79.4°
	69.0°	69.6°
	92.2°	92.3°
Zr-O-Si bond angles	99.2°	100.0°
	149.8°	151.0°
Zr-O-Zr bond angle	111.0°	110.4°

## B. The simulation method

Molecular dynamics simulations were performed using version 2.14 of the DLPOLY computer code<sup>34</sup> developed at Daresbury Laboratory, U.K. with a modification to allow the use of a variable time step. Most of the simulations were conducted with a cell consisting of  $6 \times 6 \times 6$  unit cells containing 5184 ions and a maximum time step of 1 fs. Energy conservation was within 1% of the kinetic energy. In addition, a limited number of simulations were performed with a cell consisting of  $18 \times 18 \times 18$  unit cells containing 139 968 ions to examine system size effects. The reidite structure was simulated using  $8 \times 8 \times 3$  unit cells containing 4608 ions and  $22 \times 22 \times 10$  unit cells containing 116 160 ions. Periodic

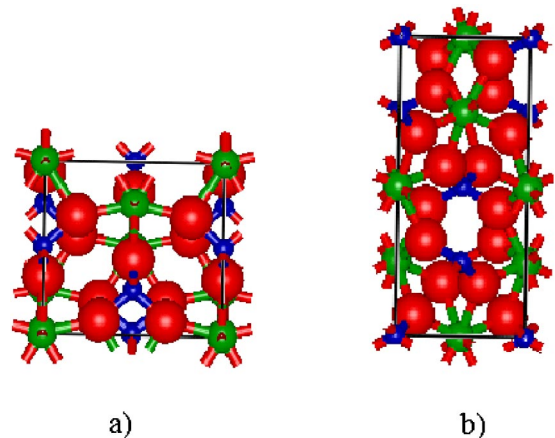


FIG. 2. The structure of (a) zircon and (b) reidite polymorphs of  $\text{ZrSiO}_4$ . The largest ion is O and the smallest is Si.

TABLE IV. Comparison between experimental data and the present zircon model.

Property	Experiment (Refs. 27–33)	Present model
Density ( $\text{kg/m}^3$ )	4662.0	4584.0
Elastic constants		
$C_{11}$ (GPa)	424.0	445.0
$C_{33}$ (GPa)	490.0	479.0
$C_{44}$ (GPa)	114.0	84.0
$C_{66}$ (GPa)	49.0	64.0
$C_{12}$ (GPa)	70.0	64.0
$C_{13}$ (GPa)	149.0	133.0
Bulk modulus (GPa)	225.0	223.0
$C_p$ at 300 K ( $\text{J mol}^{-1} \text{K}^{-1}$ )	98.6	102.1
$S$ at 300 K ( $\text{J mol}^{-1} \text{K}^{-1}$ )	84.4	84.2
Dielectric constant $\epsilon$	8–12	$\epsilon_{xx} = \epsilon_{yy} = 5.4$ $\epsilon_{zz} = 11.9$

boundary conditions were used in all the simulations. The constant NPT ensemble<sup>35</sup> was used to simulate the melting of zircon, while the amorphous state was studied in the constant NVT ensemble.<sup>36</sup> The simulation cell was initially equilibrated for 10 ps at a constant temperature and averages of various thermodynamic properties, diffusion coefficients, radial distribution functions, and bond angle distributions were determined over the next 10 to 20 ps. By determining diffusion coefficients in the melt at several temperatures, the activation energies for self diffusion have been determined.

Amorphous zircon was produced by melt quenching a simulation cell containing 5184 ions. Starting from the zircon crystal at 2000 K, the temperature was raised to 5000 K. The molar volume of the simulation cell was set 18% higher than that of the perfect crystal of zircon at 300 K. The simulation cell was equilibrated at 5000 K for 50 ps and quenched to 30 K over 10 ps by controlling the temperature of the outermost layers. This corresponds to a quench rate of the order of  $10^{15}$  K/s and is much higher than rates achieved in quenching experiments. The volume expansion was chosen

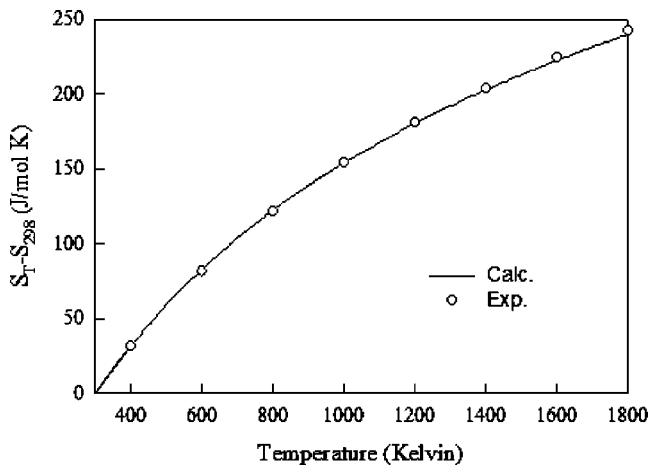
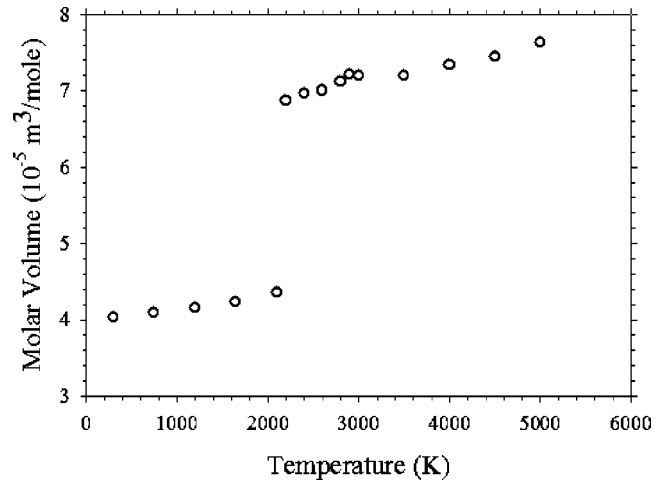
FIG. 3. Comparison between experimental (Ref. 30) and calculated entropy difference  $S_T - S_{298}$ .

FIG. 4. Temperature dependence of the molar volume of zircon.

to simulate the experimental observed swelling in amorphous zircon,<sup>4,6</sup> and be consistent with the *ab initio* simulation of Balan *et al.*<sup>19</sup> The structure of melt quenched zircon with 18% swelling was examined at 300 K in the NVT ensemble and the pressure was found to be about 8 GPa. This structure will be referred to as the low density (LD) amorphous state to be consistent with the terminology used by Balan *et al.*<sup>19</sup>

In addition to the LD amorphous state, a high density (HD) disordered state was simulated as follows in order to model a highly distorted zircon structure at the onset of amorphization. Crystalline zircon was equilibrated at 2100 K for 20 ps in the NPT ensemble and found to have a volume expansion of 8% relative to crystalline zircon at 300 K. The simulation cell was then quenched at constant volume using static layers at the boundaries and equilibrated in the NVT ensemble at 300 K for 10 ps. The computations were performed using multiple processors of a 6080 processor IBM/SP at the National Energy Research Scientific Computing Center at Lawrence Berkeley National Laboratory.

### III. RESULTS AND DISCUSSION

Figure 4 shows the simulated molar volume of zircon as a function of temperature at zero pressure. The coefficient of linear expansion at 300 K is about  $1 \times 10^{-5} \text{ K}^{-1}$ , which is larger than the experimental value.<sup>37</sup> The volume undergoes an abrupt jump between 2100 and 2200 K. The  $\text{ZrO}_2$ - $\text{SiO}_2$  phase diagram<sup>38</sup> indicates that  $\text{ZrSiO}_4$  decomposes into  $\text{ZrO}_2$ - and  $\text{SiO}_2$ -rich liquid at about 1960 K and the two-phase region extends from 1960 to 2675 K.

The radial distribution functions  $g(r)$  for zircon in the NPT ensemble at 300, 2200, and 5000 K are shown in Fig. 5. At 300 K, the  $g(r)$  shows a Si-O peak around 1.6 Å and two Zr-O peaks around 2.1 and 2.3 Å. There is clear evidence of long-range order corresponding to the zircon structure. At 2200 K, the two Zr-O distributions merge into a single broad peak and the peaks of the Si-O and Zr-O distances shift to smaller distances of about 1.55 and 1.95 Å, respectively. There is no discernible structure beyond about 4 Å, indicating that there is no long range order at this temperature. At 5000 K, the Si-O and Zr-O bond lengths are slightly shorter,

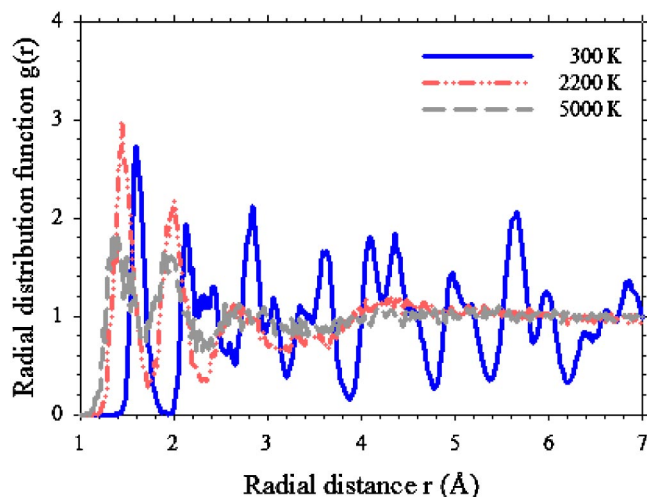


FIG. 5. Radial distribution function of zircon at 300, 2200, and 5000 K.

and at long distances, the  $g(r)$  curve overlaps the curve corresponding to 2200 K.

In an effort to understand the structural changes occurring around 2100 K, the connectivity of silicon units was determined from the number of bridging oxygens. In a perfect crystal of zircon, there are no bridging oxygens ( $Q^0$ ), while in silica there are four bridging oxygens ( $Q^4$ ). The presence of bridging oxygens is thus an indication of decomposition of  $\text{ZrSiO}_4$  into  $\text{ZrO}_2$  and  $\text{SiO}_2$ . The cutoff distances for Si-O and Zr-O bonds have been taken to be 2.7 and 3.3 Å, respectively, in the present work. These values were chosen based on the minima in the respective pair distribution functions from a large number of configurations with varying levels of volume swelling. Figure 6 represents the connectivity of Si at 2100, 2200, and 5000 K. At 2100 K, nearly 93% of Si ions are unconnected, while about 7% have one bridging oxygen. The corresponding values at 1650 K (not shown in Fig. 6) are 99.3 and 0.7%, respectively. At 2200 K, more than 50% of Si are connected, with  $Q^1$  (38.6%) and  $Q^2$  (10.5%) being

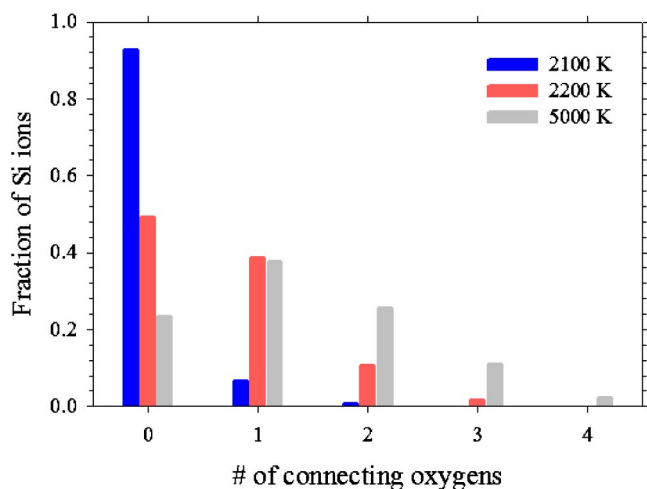


FIG. 6. The degree of polymerization of Si units in zircon at 2100, 2200, and 5000 K.

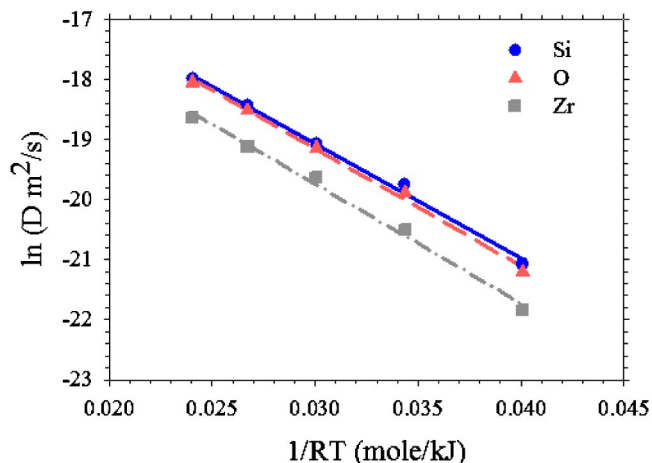


FIG. 7. Self-diffusion coefficient ( $D$ ) in molten zircon as a function of the reciprocal of temperature ( $T$ ).  $R$  is the universal gas constant.

dominant. At 5000 K, only 23.5% of Si are unconnected, with  $Q^1$  (37.7%),  $Q^2$  (25.5%),  $Q^3$  (11%), and  $Q^4$  (2.3%) accounting for the rest.

The abrupt increase in volume, loss of long range order in the radial distribution function, and significant increase in the fraction of Si connected to other Si through O bridges indicates decomposition of zircon above 2100 K. In addition, the mean square ionic displacement increases linearly with time above 2100 K, which is a clear indication of random walk or diffusive processes that are characteristic of the liquid state. This temperature is in good agreement with the experimental value of 1960 K.<sup>38</sup> Due to the lack of free surfaces and point defects in the present work, the transition temperature is overestimated and the observed temperature can be considered the upper limit of the melting temperature. A simulation cell containing 139 968 ions was examined at 300 and 2200 K in the NPT ensemble at zero applied pressure for 10 ps to compare with the above results obtained for 5184 ions. The results were identical for the two system sizes, and indicate that the observed phenomena are independent of system size. The ability of the potential to reproduce not only the elastic constants and structure but also the thermal decomposition of zircon indicates that it is well suited for the study of radiation damage in zircon leading to the disordered state.

The self-diffusion coefficient in molten zircon for each ion  $D_{\text{ion}}$  was calculated in the temperature range 3000 to 5000 K, by determining the mean square displacement  $\langle \Delta r_{\text{ion}}(t)^2 \rangle$  as a function of time  $t$  in the linear regime over times of the order of 20 to 50 ps using the equation

$$D_{\text{ion}} = \frac{1}{6} \frac{d}{dt} \langle \Delta r_{\text{ion}}(t)^2 \rangle. \quad (6)$$

The self-diffusion coefficients of Zr, Si, and O ions in zircon is plotted on a logarithmic scale as a function of the reciprocal temperature at 500 K intervals between 3000 and 5000 K in Fig. 7. The least-squares linear fit to the data is also shown. The self-diffusion coefficients of the ions are well described by an Arrhenius relationship. The preexponentials

TABLE V. Pre-exponential  $D_0$  and activation energies  $Q$  for self-diffusion in molten  $\text{ZrSiO}_4$ 

Ion	$D_0$ ( $10^{-6}$ m <sup>2</sup> /s)	$Q$ (kJ/mole)
Zr	1.01	198.1
Si	1.58	190.3
O	1.66	195.0

and activation energies for diffusion are shown in Table V. Direct experimental data on self-diffusion in molten zircon is unavailable, which precludes a reliable comparison with experiment. The calculated values are nevertheless consistent with the first stage of recrystallization of partially metamict zircon identified by Giesler *et al.*<sup>39</sup> as driven by point defect annealing with an activation energy of 212 kJ/mole. Furthermore, the diffusion coefficients obtained in the present work are broadly consistent with experimentally determined self-diffusivities of Si and O in silicate melts.<sup>40–41</sup>

In addition to studying the thermal decomposition of zircon, the relative stability of zircon and reidite (high pressure polymorph) were examined by simulating the reidite structure in the NVT ensemble at 300 K and the NPT ensemble at 300 K with zero applied pressure. Reidite cells containing 4608 and 116 160 ions, respectively, were simulated with lattice constants  $a = 4.738$  and  $c = 10.506$  Å corresponding to a density of 5161 kg/m<sup>3</sup>. In the NVT ensemble at 300 K, the potential energy of reidite was about 133 kJ/mole higher than that of zircon, and the pressure on the cell was about 17 GPa. The experimentally documented<sup>26</sup> athermal transformation from reidite to zircon was not observed in the present work. Instead, when reidite was allowed to relax at zero pressure and 300 K in the NPT ensemble, it transformed into an amorphous state with a volume swelling of about 42%, but comparable to the LD state as far as the Si-O and Zr-O distributions, and the lack of long-range order are concerned. The LD state has a potential energy about 15–30 kJ/mole higher than that of crystalline zircon, depending on the swelling and level of relaxation of the amorphous state. Thus, there exists a large driving force of nearly 100 kJ/mole for reidite to transform to the LD amorphous state. The thermodynamic properties of the reidite state and the occurrence of the reidite to LD amorphous transformation were found to be independent of system size.

Figure 8 shows the radial distribution functions (RDF's) for the HD and LD disordered states. The peak in the Si-O distribution is at about 1.48 and 1.54 Å in the LD and HD states, respectively. The peak in the Zr-O distribution occurs at 2.0 and 2.2 Å in LD and HD disordered states, respectively. The corresponding experimentally determined value in metamict zircon is about 2.14 Å.<sup>42</sup> These distributions are narrow in the LD state and broader in the HD state. The LD state has no long-range order, while the HD state is disordered but retains peaks characteristic of the zircon structure as is evident by comparing Fig. 8 and Fig. 5. The average Si coordination is about 3.5 and average Zr coordination is about 7 in the LD state. The latter value reproduces well the experimental Zr coordination of 6.8–7.2 in metamict

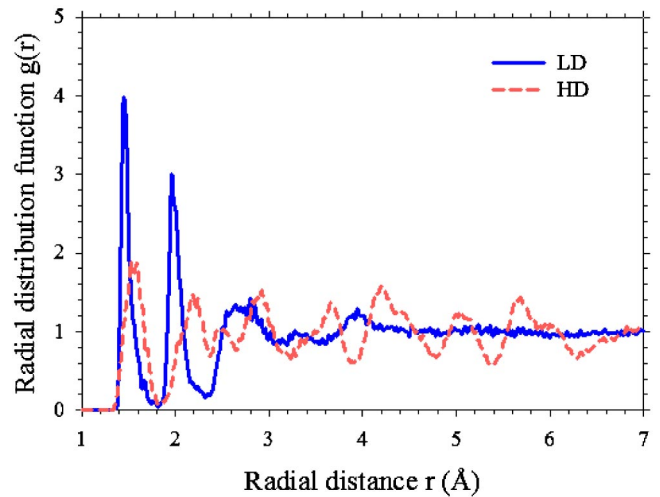


FIG. 8. Radial distribution function of the high density (HD) and low density (LD) disordered states of zircon.

zircon.<sup>42</sup> The Si and Zr coordination numbers in the HD disordered state are 4 and 8, respectively, as is the case for crystalline zircon.

The connectivity of Si units in LD amorphous and HD disordered states is shown in Fig. 9. The average polymerization of Si in the LD amorphous state is 1.95, while it is 0.04 in the HD state. The decreased coordination of Zr, the shortening of the Zr-O bond, and the average polymerization of Si units in the LD amorphous state are all consistent with recent *ab initio* molecular dynamics simulations<sup>19</sup> and experimental XAS (Ref. 10) and Raman studies.<sup>11</sup> However, the Si-O bond distance of about 1.48–1.56 Å observed in the present work for disordered states is shorter than the value of 1.68 Å observed in *ab initio* calculations.<sup>19</sup>

Figure 10 shows the pair distribution functions, which represent the probability of finding a given pair of ions weighted by the atomic numbers, for Zr-Zr, Zr-Si, and Si-Si pairs in the HD disordered state. These pair distributions, and the coordination numbers of Zr and Si, are similar to those

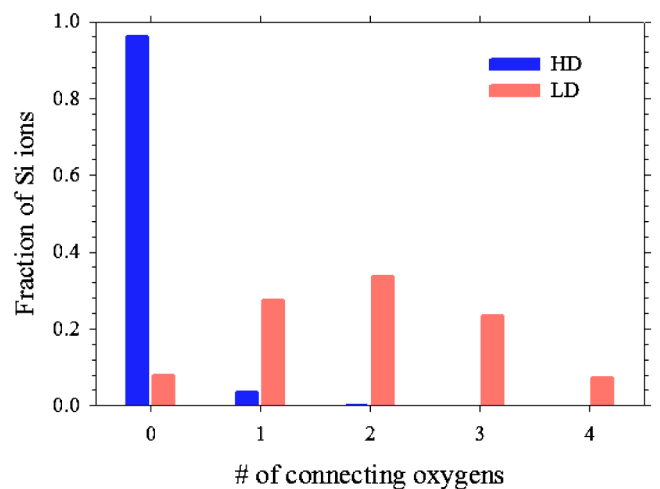


FIG. 9. The degree of polymerization of Si units in high density (HD) and low density (LD) states.

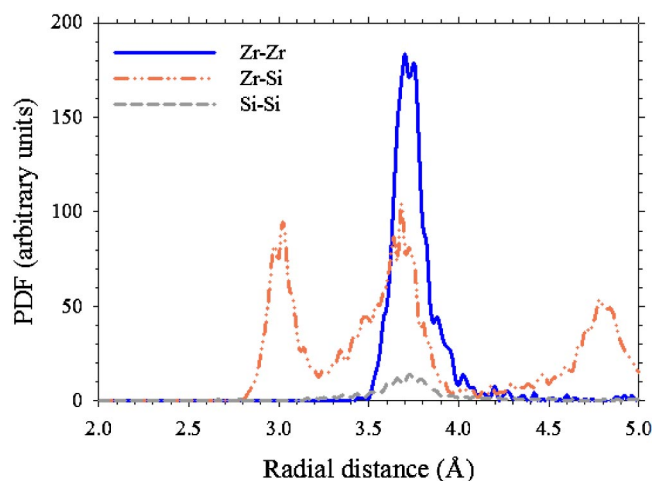


FIG. 10. Pair distribution functions, weighted by atomic numbers of interacting species, in the high density state.

determined experimentally by Begg *et al.*<sup>6</sup> in synthetic zircon amorphized by the decay of incorporated <sup>238</sup>Pu. The occurrence of a single Zr-O peak at 2.2 Å in the pair distribution function (not shown in Fig. 10) is also consistent with the results of Begg *et al.*<sup>6</sup> The HD disordered state was found to have a potential energy of about 20 kJ/mole higher than the perfect crystal, while the corresponding value for the LD amorphous state is between 15 and 30 kJ/mole. These values are smaller than the 59 kJ/mole value of enthalpy of annealing of metamict zircon determined by calorimetry.<sup>43</sup>

The structure of HD and LD states was further examined by comparing the distributions of O-Si-O bonds and Zr-O-Si bonds in HD and LD states with those for crystalline zircon equilibrated at 300 K. These are shown in Figs. 11 and 12, respectively. In crystalline zircon, the O-Si-O distribution shows sharp peaks at 97° and 116°, while the Zr-O-Si distribution shows peaks at 100° and 151°, as indicated in Table III. The O-Si-O peaks become broader and start to overlap in the HD state, while the LD state shows a very broad distribution with a peak at about 120°. The Zr-O-Si

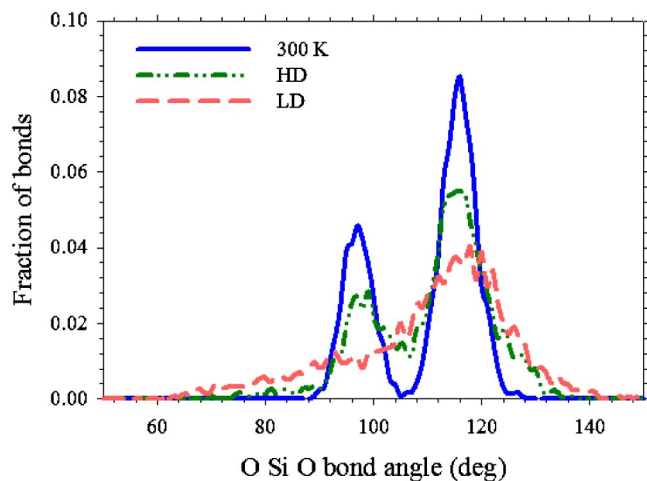


FIG. 11. O-Si-O bond angle distribution in crystalline zircon at 300 K, HD disordered state, and LD amorphous state.

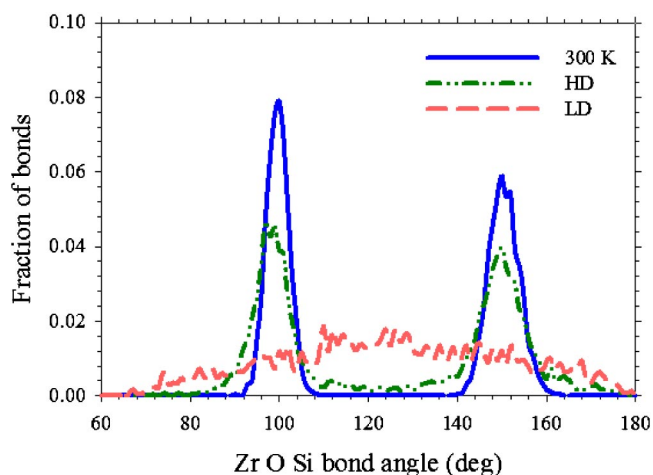


FIG. 12. Zr-O-Si bond angle distribution in crystalline zircon at 300 K, HD disordered state, and LD amorphous state.

also shows this progressive broadening of the bond angle distribution in going from the crystal to the HD state and then the LD state.

In order to examine the role of volume expansion in the crystalline-to-amorphous transformation of zircon, the HD state was isotropically expanded at 300 K in the NVT ensemble. After a small expansion of the HD state, corresponding to 10% volume swelling relative to the perfect crystal, the transformation to the LD amorphous state occurred. The peak of the Zr-O and Si-O bond length distributions shifted to lower values of 2 and 1.48 Å, respectively. The Zr and Si coordination numbers decreased to about 7.2 and 3.6, respectively. Nearly 10% of the Si showed  $Q^1$  connectivity and a further 2%  $Q^2$  connectivity indicating an increase in Si polymerization. The energy of the system decreased by about 3 kJ/mole during this transformation. These results indicate that the HD state represents a critical volume expansion beyond which crystalline zircon becomes thermodynamically unstable with respect to the amorphous state. This is consistent with the fact that the HD state is obtained by quenching from crystalline zircon heated to a temperature just below the onset of melting. Furthermore, experimental results<sup>4</sup> from natural zircon indicate that the volume expansion of the crystalline regions of the sample increases with dose and saturates at about 4–6% for a dose of 0.15–0.3 dpa. The contribution of the crystalline fraction dominates the total macroscopic swelling up to a dose of 0.15 dpa. At higher doses, the amorphous fraction increases rapidly with dose, suggesting that there is a limit beyond which volume expansion of the crystal leads to amorphization.

The present simulations are consistent with the generalized Lindemann melting criterion<sup>44–46</sup> that is based on parallels between melting and solid state amorphization. Wolf *et al.*<sup>44</sup> proposed a thermodynamics-based description of melting and solid-state amorphization, according to which volume expansion is the underlying cause of disordering in both phenomena. Beyond a critical volume expansion, the disordered crystal becomes thermodynamically unstable with respect to the amorphous state. Okamoto and co-workers<sup>45,46</sup> have proposed that the sum of the dynamic and static root-

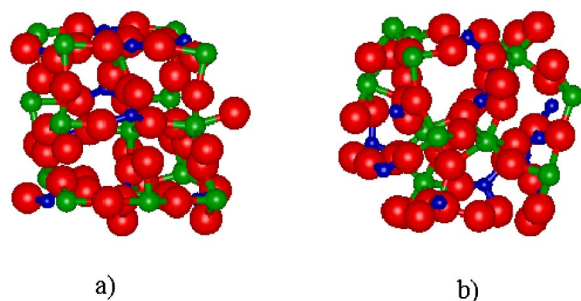


FIG. 13. Structure of (a) high density and (b) low density disordered states. The largest ion is O, and the smallest is Si.

mean-square atomic displacements expressed as a fraction of the nearest-neighbor distance is a better indicator of mechanical instability than volume expansion, critical strain, or atomic level stress. According to this model, the crystalline-to-amorphous transition can be viewed as disorder-induced melting of a defective crystal occurring at temperatures below the ideal glass transition temperature.

In the present work, the HD state represents the disordered crystal at the onset of amorphization, while the LD state is comparable to fully amorphous zircon. This is evident from Fig. 13, which shows a small section of the simulation cell for HD and LD states. In the HD state, the bonds are distorted and bond lengths are different when compared to the perfect crystal, but the  $\text{ZrO}_8$  and  $\text{SiO}_4$  units are intact. When the level of disorder increases beyond the critical value represented by the HD state, zircon transforms to the LD state with substantial distortion of bonds. This amorphization is accompanied by a decrease in the average Zr coordination number, increase in the polymerization of Si units, distortion of O-Si-O and Zr-O-Si bonds, formation of Zr-O-Zr linkages, and loss of long-range order in agreement with previous studies.<sup>10-11,19</sup>

#### IV. CONCLUSIONS

The thermal decomposition of zircon and the structure of disordered states of zircon have been simulated by molecular dynamics using a newly developed partial charge model that reproduces the structure, elastic properties, and thermal decomposition of zircon. The activation energy for self-diffusion in the liquid was found to be about 190 kJ/mole in reasonable agreement with experimental data from silicate melts. Two disordered states were simulated to model metamict zircon. A high density disordered state with minimal Si polymerization, bond distortion, and a volume swelling of 8% was found to correspond to a distorted zircon crystal at the onset of amorphization. A low density amorphous state with a volume swelling of 18%, average polymerization of  $Q^2$ , reduced Zr coordination, and considerable bond distortion matched the structure observed experimentally in metamict natural zircon. These results, when viewed in light of experimental findings in irradiated zircon, suggest that at low doses, the damage in zircon is accommodated within the crystal lattice. This disordered crystal becomes thermodynamically unstable with respect to the amorphous state as the volume expansion increases with dose.

#### ACKNOWLEDGMENTS

This research was supported by the Division of Materials Sciences and Engineering, Office of Basic Energy Sciences, U.S. Department of Energy under Contract No. DE-AC06-76RLO 1830. It used resources of the National Energy Research Scientific Computing Center, which is supported by the Office of Science of the U.S. Department of Energy under Contract No. DE-AC03-76SFO 0098.

\*Electronic address: ram.devanathan@pnl.gov

<sup>1</sup>R. C. Ewing, Proc. Natl. Acad. Sci. U.S.A. **96**, 3432 (1999).

<sup>2</sup>R. C. Ewing, W. Lutze, and W. J. Weber, J. Mater. Res. **10**, 243 (1995).

<sup>3</sup>E. B. Anderson, B. E. Burakov, and E. M. Pazhukin, Radiochim. Acta **60**, 149 (1993).

<sup>4</sup>W. J. Weber, R. C. Ewing, and L. M. Wang, J. Mater. Res. **9**, 688 (1994).

<sup>5</sup>G. D. Wilk, R. M. Wallace, and J. M. Anthony, J. Appl. Phys. **89**, 5243 (2001).

<sup>6</sup>B. D. Begg, N. J. Hess, W. J. Weber, S. D. Conradson, M. J. Schweiger, and R. C. Ewing, J. Nucl. Mater. **278**, 212 (2000).

<sup>7</sup>A. Meldrum, L. A. Boatner, and R. C. Ewing, Phys. Rev. B **56**, 13 805 (1997).

<sup>8</sup>E. K. H. Salje, J. Chrosch, and R. C. Ewing, Am. Mineral. **84**, 1107 (1999).

<sup>9</sup>E. R. Vance, Radiat. Eff. **24**, 1 (1975).

<sup>10</sup>J. A. Woodhead, G. R. Rossman, and L. T. Silver, Am. Mineral. **76**, 74 (1991).

<sup>11</sup>F. Farges and G. Calas, Am. Mineral. **76**, 60 (1991).

<sup>12</sup>M. Zhang, E. K. H. Salje, I. Farnan, A. Graeme-Barber, P. Daniel,

R. C. Ewing, A. M. Clark, and H. Leroux, J. Phys.: Condens. Matter **12**, 1915 (2000).

<sup>13</sup>I. Farnan and E. K. H. Salje, J. Appl. Phys. **89**, 2084 (2001).

<sup>14</sup>A. Meldrum, S. J. Zinkle, L. A. Boatner, and R. C. Ewing, Phys. Rev. B **59**, 3981 (1999).

<sup>15</sup>R. E. Williford, W. J. Weber, R. Devanathan, and A. N. Cormack, J. Nucl. Mater. **273**, 164 (1999).

<sup>16</sup>B. Park, W. J. Weber, and L. R. Corrales, Phys. Rev. B **64**, 174108 (2001).

<sup>17</sup>K. Trachenko, M. T. Dove, and E. K. H. Salje, J. Phys.: Condens. Matter **13**, 1947 (2001).

<sup>18</sup>J. P. Crocombette and D. Ghaleb, J. Nucl. Mater. **295**, 167 (2001).

<sup>19</sup>E. Balan, F. Mauri, C. Pickard, I. Farnan, and G. Calas, Am. Mineral. **88**, 1769 (2003).

<sup>20</sup>C. Meis and J. D. Gale, Mater. Sci. Eng., B **57**, 52 (1998).

<sup>21</sup>M. J. Akhtar and S. Waseem, Chem. Phys. **274**, 109 (2001).

<sup>22</sup>U. Essmann, L. Perera, M. L. Berkowitz, T. Darden, H. Lee, and L. G. Pedersen, J. Chem. Phys. **103**, 8577 (1995).

<sup>23</sup>J. D. Gale, J. Chem. Soc., Faraday Trans. **93**, 629 (1997).

<sup>24</sup>J. F. Ziegler, J. P. Biersack, and U. Littmark, *The Stopping and Range of Ions in Matter* (Pergamon Press, New York, 1985).

- <sup>25</sup>K. Robinson, G. V. Gibbs, and P. H. Ribbe, *Am. Mineral.* **56**, 782 (1971).
- <sup>26</sup>B. P. Glass, S. Liu, and P. B. Leavens, *Am. Mineral.* **87**, 562 (2002).
- <sup>27</sup>H. Özkan, L. Cartz, and J. C. Jamieson, *J. Appl. Phys.* **45**, 556 (1974).
- <sup>28</sup>J. A. Speer, *Reviews in Mineralogy* (Mineralogical Society of America, Chelsea, MI, 1982), Vol. 5.
- <sup>29</sup>R. C. Ewing, *J. Mater. Res.* **10**, 243 (1995).
- <sup>30</sup>J. P. Coughlin and E. G. King, *J. Am. Chem. Soc.* **72**, 2262 (1950).
- <sup>31</sup>F. Gervais, B. Piriou, and F. Cabannes, *J. Phys. Chem. Solids* **34**, 1785 (1973).
- <sup>32</sup>C. Pecharroman, M. Ocana, P. Tartaj, and C. J. Serna, *Mater. Res. Bull.* **29**, 417 (1994).
- <sup>33</sup>A. F. Wells, *Structural Inorganic Chemistry* (Oxford University Press, Oxford, 1984).
- <sup>34</sup>W. Smith and T. R. Forester, *J. Mol. Graphics* **14**, 136 (1996).
- <sup>35</sup>S. Melchionna, G. Ciccotti, and B. L. Holian, *Mol. Phys.* **78**, 533 (1993).
- <sup>36</sup>W. G. Hoover, *Phys. Rev. A* **31**, 1695 (1985).
- <sup>37</sup>S. L. Chaplot, R. Mittal, E. Busetto, and A. Lausi, *Phys. Rev. B* **66**, 064302 (2002).
- <sup>38</sup>W. Butterman and W. R. Foster, *Am. Mineral.* **52**, 880 (1967).
- <sup>39</sup>T. Geisler, R. T. Pidgeon, W. van Brouswijk, and R. Pleysier, *Eur. J. Mineral.* **13**, 1163 (2001).
- <sup>40</sup>D. Tinker and C. E. Leshner, *Am. Mineral.* **86**, 1 (2001).
- <sup>41</sup>C. E. Leshner, R. L. Hervig, and D. Tinker, *Geochim. Cosmochim. Acta* **60**, 405 (1996).
- <sup>42</sup>F. Farges, *Phys. Chem. Miner.* **20**, 504 (2001).
- <sup>43</sup>S. Ellsworth, A. Navrotsky, and R. C. Ewing, *Phys. Chem. Miner.* **21**, 140 (1994).
- <sup>44</sup>D. Wolf, P. R. Okamoto, S. Yip, J. F. Lutsko, and M. Kluge, *J. Mater. Res.* **5**, 286 (1990).
- <sup>45</sup>P. R. Okamoto, N. Q. Lam, and L. E. Rehn, in *Solid State Physics*, edited by H. Ehrenreich and F. Spaepen (Academic, Boston, 1999), Vol 52, p. 1.
- <sup>46</sup>P. C. Liu, P. R. Okamoto, N. J. Zaluzec, and M. Meshii, *Phys. Rev. B* **60**, 800 (1999).